

de Gennes Narrowing and the Relationship Between Structure and Dynamics in Self-Organized Ion Beam Nanopatterning

Peco Myint*

*Division of Materials Science and Engineering,
Boston University, Boston, Massachusetts 02215 USA*

Karl F. Ludwig, Jr.†

*Department of Physics and
Division of Materials Science and Engineering,
Boston University, Boston, Massachusetts 02215 USA*

Lutz Wiegart, Yugang Zhang, and Andrei Fluerasu

*National Synchrotron Light Source II,
Brookhaven National Lab, Upton, NY 11973 USA*

Xiaozhi Zhang and Randall L. Headrick

*Department of Physics and Materials Science Program,
University of Vermont, Burlington, Vermont 05405 USA*

(Dated: May 1, 2022)

Investigating the relationship between structure and dynamical processes is a central goal in condensed matter physics. Perhaps the most noted relationship between the two is the phenomenon of de Gennes narrowing, in which relaxation times in liquids are proportional to the scattering structure factor. Here a similar relationship is discovered during the self-organized ion beam nanopatterning of silicon using coherent x-ray scattering. However, in contrast to the exponential relaxation of fluctuations in classic de Gennes narrowing, the dynamic surface exhibits a wide range of behavior as a function of length scale, with a compressed exponential relaxation at lengths corresponding to the dominant structural motif - self-organized nanoscale ripples. These behaviors are reproduced in simulations of a nonlinear model describing the surface evolution. We suggest that the compressed exponential behavior observed here is due to the morphological persistence of the self-organized surface ripple patterns which form and evolve during ion beam nanopatterning.

Understanding the relationship between structure and dynamical processes is a central goal in condensed matter physics. Coherent x-ray scattering has emerged as a powerful approach which can simultaneously investigate dynamics through X-ray Photon Correlation Spectroscopy (XPCS) and structure through measurement of the scattering structure factor [1, 2]. The quintessential relationship between fluctuation dynamics and structure is the phenomenon of de Gennes narrowing, in which the neutron inelastic scattering linewidth $w(q)$ in liquids is found to narrow at the position of the peak in the scattering structure factor $I(q)$, with $w(q) \sim I(q)^{-1}$ [3]. The corresponding correlation times $\tau(q)$ are then proportional to $I(q)$. Here we use coherent x-ray scattering to explore the relation between structure and dynamics during the phenomenon of self-organized ion beam nanopatterning and find telling similarities with de Gennes narrowing, but also important differences. Simulations of the surface evolution are shown to reproduce the observed behavior which we relate to the evolving ripple morphology on the surface.

Coherent scattering experiments measure dynamics in the time domain through correlation functions, particularly the intensity autocorrelation $g_2(\mathbf{q}, \Delta t) = \langle I(\mathbf{q}, t_1)I(\mathbf{q}, t_2) \rangle_{t'} / \langle I(\mathbf{q}, t') \rangle_{t'}^2$, where $\Delta t = |t_1 - t_2|$ and t' represents the range in t_1 and t_2 times over which the function is calculated[4]. For a practical matter, this function is also typically averaged over equivalent values of \mathbf{q} . While the detailed behavior of the correlation function can be complex, experimentally they can often be fit with a Kohlrausch-Williams-Watts (KWW) function [5]: $g_2(\mathbf{q}, \Delta t) = \{1 + \beta \exp[-2(\Delta t/\tau(\mathbf{q}))^{n(\mathbf{q})}]\}$, where $n(\mathbf{q})$ is an exponent characterizing the fluctuation decay and β is an experimental contrast factor. In a simple linear process with uncorrelated Gaussian random noise $\eta(\mathbf{q}, t)$, the evolution of the spatially-dependent system ordering $\phi(\mathbf{q}, t)$ is:

$$\frac{\partial \phi(\mathbf{r}, t)}{\partial t} = -A(\mathbf{q})\phi(\mathbf{q}, t) + \eta(\mathbf{q}, t). \quad (1)$$

If $A(\mathbf{q})$ is positive so that the system is stable to fluctuations, then, in equilibrium, the structure factor intensity is $\langle I(\mathbf{q}) \rangle \sim \langle \phi^*(\mathbf{q}, t)\phi(\mathbf{q}, t) \rangle \sim \langle \eta^2 \rangle / A(\mathbf{q})$. The intensity autocorrelation function $g_2(\mathbf{q}, \Delta t)$ exhibits an exponential decay with time constant $1/2A(\mathbf{q})$ [6] so that $\tau(\mathbf{q}) \sim \langle I(\mathbf{q}) \rangle$. Thus, the classic de Gennes relationship

* peco@bu.edu

† ludwig@bu.edu

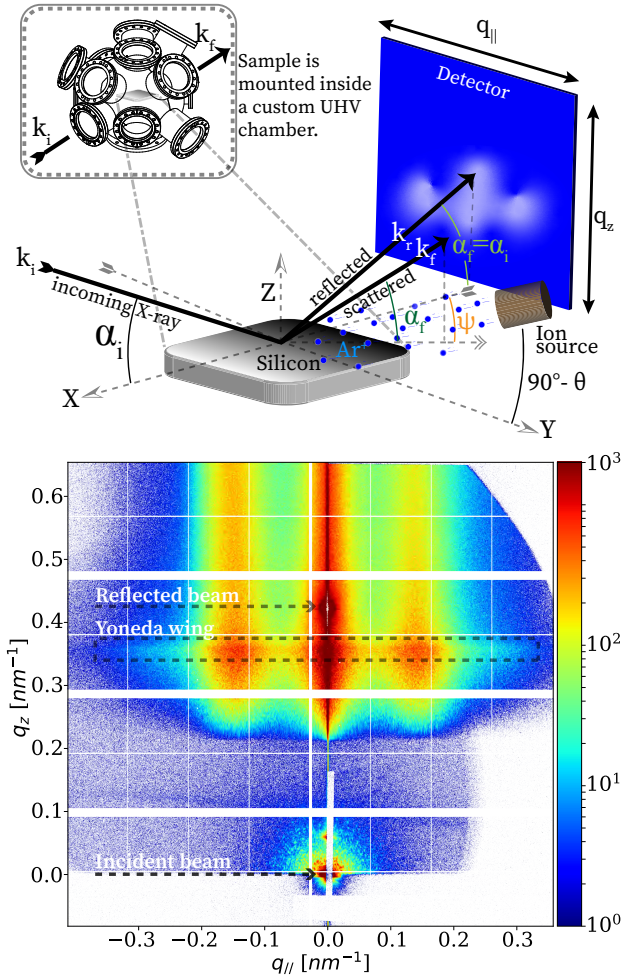


FIG. 1. Top: A schematic diagram of the GISAXS experiment. The ion source is placed at the polar angle θ , which causes self-organized rippling on the silicon surface. The sample is positioned so that the X-ray incident angle α_i is slightly above the critical angle of total external reflection. The scattering is recorded as a function of the exit angles α_f and ψ using a 2D detector. Bottom: A detector image during nanopatterning. The Yoneda wing, spread across $q_z = 0.36 \text{ nm}^{-1}$ or $q'_z = 0.16 \text{ nm}^{-1}$, is the surface-sensitive scattering exiting the sample at the critical angle, α_c . For Ar^+ patterning, correlation peaks at q_{\parallel} or $q_0 \simeq \pm 0.18 \text{ nm}^{-1}$ are due to the correlated nanoripples on the surface.

is a hallmark of a purely linear dynamics. If the dynamics contains nonlinearities then the relaxation is no longer exponential and the deviation of the KWW exponent $n(q)$ provides an important characterization of the nonlinear behavior.

This study uses coherent Grazing-Incidence Small-Angle X-ray Scattering (co-GISAXS) to investigate the nanopatterning dynamics during 1 keV Ar^+ and Kr^+ ion bombardment of silicon at an angle of $\theta = 65^\circ$. At this bombardment angle, nano-ripples are known to form on the surface with a wavevector parallel to the projected di-

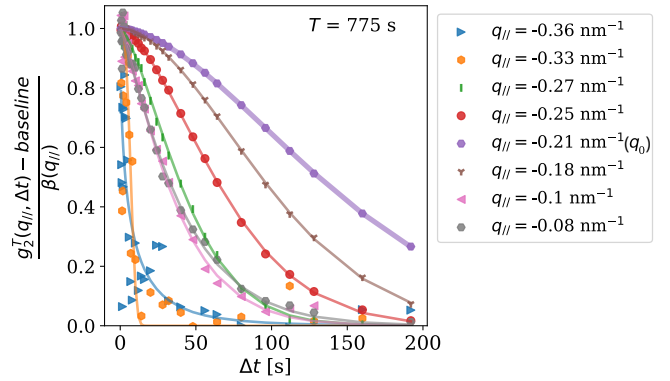


FIG. 2. KWW fits of $g_2^T(q_{\parallel}, \Delta t)$ for select wavenumbers at aging time $T=775 \text{ s}$. For Kr^+ patterning, correlation peaks are at q_{\parallel} or $q_0 \simeq \pm 0.21 \text{ nm}^{-1}$.

rection of the incoming ions onto the sample surface [7, 8]. Experiments used a photon energy of 9.65 keV and the incident X-ray angle α_i was 0.26° , which is slightly above the critical angle of total external reflection. Detector images were recorded every 0.25 s. In the x-ray scattering, the direction parallel to the ripple wavevector is denoted q_{\parallel} and the direction perpendicular to the surface is q_z . These correspond approximately with the horizontal and vertical directions on the position-sensitive x-ray detector (Fig. 1). Ions enter from the side of the positive y -axis.

We focus primarily on x-ray scattering intensity along the Yoneda wing, which is particularly sensitive to surface morphology [9]. In the limit that $q_z h$ is small, where h is a height on the surface, the GISAXS intensity along the Yoneda wing is proportional to the height-height structure factor [10]. As h becomes larger, the scattering intensity is closely related to the height-height structure factor, but reduced by destructive interference within structures. As shown in the bottom part of Fig. 1, during bombardment correlation peaks grow in the scattering pattern at wavenumbers $\pm q_0$; these are due to the formation of the correlated nano-ripples with wavelength $\lambda = 2\pi/q_0$. The ripple structure coarsens with time, but at a very slow rate so that the correlation peaks remain well within the detector window throughout the experiment. For our purposes here, this is an important difference with previous XPCS studies of ion beam nanopatterning of GaSb [11] and SiO_2 [12]. It's known that the ripples move across the surface during continued bombardment and that, at late times, the sinusoidal ripples develop into asymmetric sawtooth structures [13–16], which creates asymmetry in the scattering between positive and negative q_{\parallel} [8, 17].

To quantitatively analyze the evolution, age-dependent correlation functions $g_2^T(q_{\parallel}, \Delta t)$ with the range t' over which the autocorrelation function is evaluated being $\pm 125 \text{ s}$ around a central aging time $T = (t_1 + t_2)/2$ [18]. These were fit with the KWW form to deter-

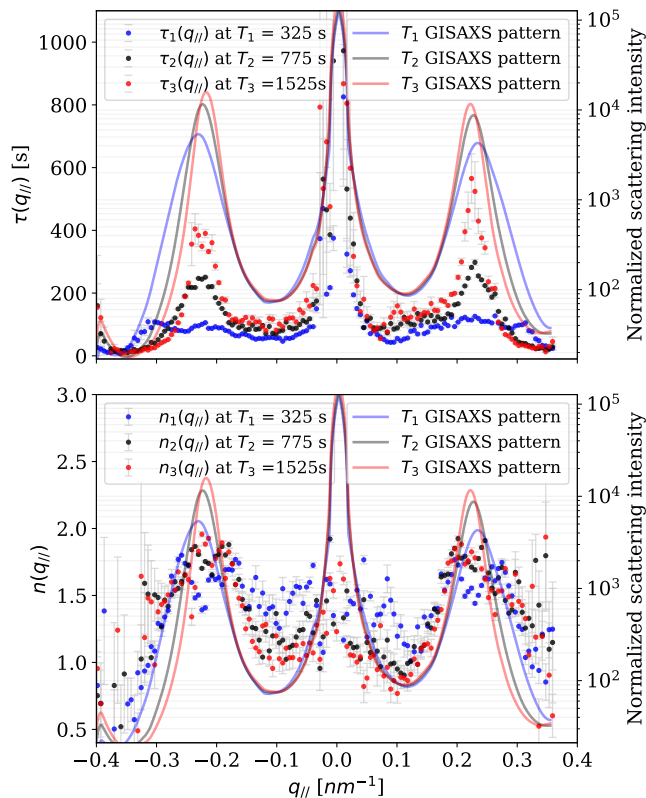


FIG. 3. Correlation times $\tau(q_{||})$ and exponents $n(q_{||})$ extracted from g_2^T fits at different aging times T for Kr^+ patterning.

mine age-dependent correlation times $\tau(q_{||})$ and exponents $n(q_{||})$. Figure 2 shows examples of the normalized $g_2^T(q_{||}, \Delta t)$ data and fits at various negative wavenumbers for $T = 775$ s. A clear change from compressed exponential behavior ($n > 1$) near the ripple wavenumber $q_0 \simeq -0.21 \text{ nm}^{-1}$ (as evidenced by downward curvature at $\Delta t = 0$) to stretched exponential behavior ($n < 1$ at high wavenumbers (as evidenced by upward curvature at $\Delta t = 0$) is observed.

Figure 3 exhibits how $\tau(q_{||})$ and $n(q_{||})$ evolve with T for Kr^+ bombardment, in comparison with the speckle-averaged scattering itself which shows peaks due to the continued growth and coarsening of correlated ripple structures. At the earliest times shown, there is only a modest variation of $\tau(q_{||})$ with wavenumber for $|q_{||}| < 0.32 \text{ nm}^{-1}$. With continued evolution, $\tau(q_{||})$ grows markedly at the ripple wavenumber, forming an increasingly narrow peak. The speckle-averaged intensity $I(q_{||})$ is slightly higher at negative $q_{||}$ than at positive $q_{||}$, while $\tau(q_{||})$ behaves in the opposite manner. Figure 3 also shows that the KWW exponent $n(q_{||})$ exhibits rich behavior, developing a peak near the ripple wavenumber with a maximum value of approximately 1.7-1.8, but falling to a value well below one at high wavenumbers.

To better understand the observed behavior, we have

performed simulations of a nonlinear model describing ion beam nanopatterning due to Harrison, Pearson and Bradley (HPB) [16, 19]:

$$\frac{\partial h(\mathbf{r}, t)}{\partial t} = A h_y + \nu_x h_{xx} + \nu_y h_{yy} + \lambda_x h_x^2 + \lambda_y h_y^2 + \gamma_y h_y^3 - \kappa \nabla^4 h + \eta(\mathbf{r}, t). \quad (2)$$

where $\eta(\mathbf{r}, t)$ is a Gaussian white noise and the individual coefficients are related to detailed surface response via sputter erosion and lateral mass redistribution. The first derivative term is related to the angle-dependence of the sputter yield and drives structures across the surface. In our case, the curvature coefficients $\nu_y < 0$, $\nu_x > 0$, so that the initial surface is unstable to the formation of ripples in the y -direction, which is the direction probed by the x-ray experiments. The effect of the quadratic terms is to control the exponential growth of the instability, while the h_y^3 term causes the initial sine-wave ripple structure to evolve into an asymmetric sawtooth structure and to coarsen. Numerical integrations were performed on a 2048×2048 lattice and, for comparison with experiment, the lattice size and time units in the simulations are set as 1 nm and 1 s respectively. Coefficients used in the simulations were chosen to reasonably model the Ar^+ bombardment: $A = -0.26$, $S_x = 0.45$, $S_y = -0.45$, $B = 6.96$, $\lambda_x = 1.94$, $\lambda_y = 1.94$, $\gamma_y = 11.89$, $\langle \eta^2 \rangle = 0.1$.

Predicted GISAXS scattered intensities $I_{sim}(q_{||})$ were calculated from the simulations using the formalism of Sinha *et al.* [10]. From these, intensity autocorrelation functions $g_{2-sim}^T(q_{||}, t)$ were calculated and fit to determine $\tau_{sim}(q_{||})$ and $n_{sim}(q_{||})$ at $T = 750$ s. These are shown in Fig. 4. Good overall agreement with the experimental trends is observed. In particular, an asymmetry in $I(q)$ develops, with the peak being slightly higher on the left than on the right side. This effect can also be calculated directly from asymmetric sawtooth patterns when the slope is higher on the positive side (ion beam) side of the sawtooth than on the negative side. This is indeed what is observed in analysis of *post-facto* AFM images and is consistent with literature results. In addition, $\tau_{sim}(q_{||})$ shows peaks at the ripple wavenumbers $\pm q_0$ and their harmonics $\pm 2q_0$, as does the exponent $n(q_{||})$.

The correlation between peaks in the scattering intensity and in $\tau(q_{||})$ found in the nanopatterning experiments and simulation is evocative of the relation between structure and dynamics embodied in de Gennes narrowing. That phenomenon is often explained physically as being due to the stability of nearest-neighbor atomic arrangements in liquids which give rise to the first sharp diffraction peak. Based upon MD simulations, however, Wu *et al.* [20] have argued that the physical cause of the phenomenon is more complex and involves correlations at long length scales for which structural rearrangements occur only slowly. In the case of ion beam nanopatterning, the obvious interpretation of the long correlation times near the ripple wavenumber q_0 is that they are due to the long-lived nature of the surface ripples.

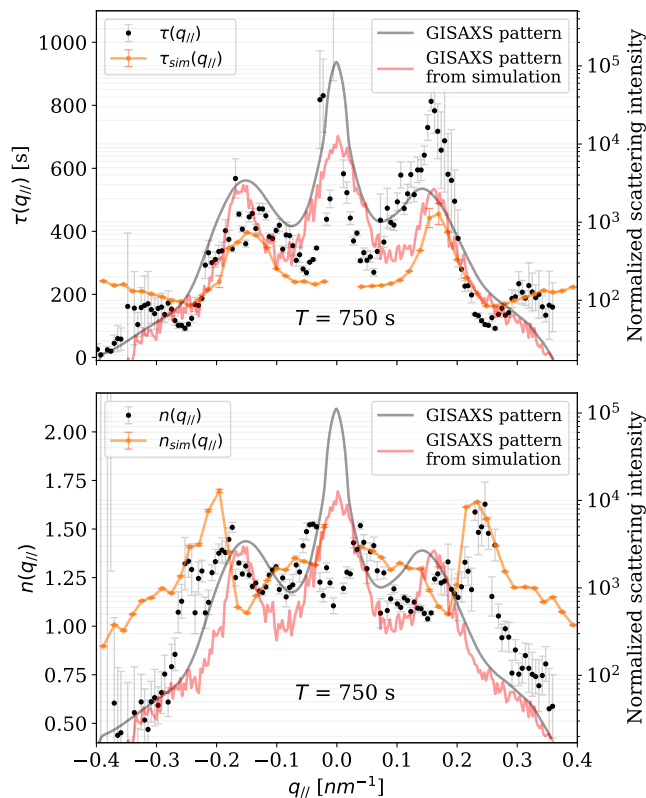


FIG. 4. Correlation times $\tau(q_{||})$ and exponents $n(q_{||})$ extracted from g_2^T fits in Ar^+ patterning and its simulation.

While the correlation time and scattering intensity are simply proportional in classic de Gennes narrowing, in the present case the relative variation in $\tau(q_{||})$ is much less than the relative variation in $I(q_{||})$ as Fig. 3 shows. Concomitantly, $g_2^T(q_{||}, \Delta t)$ near the ripple wavenumber exhibits strongly compressed exponential behavior.

Contrary to their late-time behavior, for times $\Delta t < \tau$ a compressed exponential is a *slower* decay than a simple or stretched exponential having the same time constant. The limiting slope of the KWW function as $\Delta t \rightarrow 0$ is proportional to $(\Delta t)^{n-1}$, so that stretched exponential behavior at early times requires a large contribution from short decay times, while a compressed exponential behavior $n > 1$ at early times suggests their absence [21].

The most common rationale cited for structural persistence causing compressed exponential behavior at short times Δt in both soft materials [22] and metallic glasses [23] is collective ballistic flow of local structures due to internal stress relaxation. The HPB equation, which reproduces the experiments well, does not contain any stress-related mechanism. A useful analogy is instead with the behavior of phase ordering and phase separating systems [24–28]. There, the correlation function can be calculated

from theory. Though the theoretical form for the decay of correlations involves modified Bessel functions, the KWW function fits the functional form well for $\Delta t < 2\tau$ and gives a compressed exponential with $n \approx 1.56$ and $n \approx 1.69$ for 2- and 3-dimensions respectively. For the phase ordering and phase separating systems the compressed exponent is linked to the persistence of the domain structure [24, 25]. In analogy, for self-organized ion beam nanopatterning, we suggest that the compressed exponential dynamics observed here near $\pm q_0$ points to the local morphological stability of their ripple pattern even as it moves across the surface. At higher wavenumbers $|q| > q_0$, the KWW exponent decreases to one and below, suggesting that this persistence does not exist on shorter length scales, instead there is a range of relaxation rates, including some that are quite short.

From these perspectives, it's also noteworthy that the HPB equation includes the Kardar-Parisi-Zhang (KPZ) quadratic nonlinearities h_x^2, h_y^2 [29]. The results for the pattern-forming ion bombardment process can be compared with the behavior of the KPZ equation itself, which exhibits only kinetic roughening without the formation of ordered structures. In (2+1) dimensions, the equilibrium KPZ intensities scale as $I(q) \sim q^{-(2+2\alpha)}$ while relaxation times scale as $\tau(q) \sim q^{-z}$, where $\alpha \approx 0.39$ is the roughness exponent and $z \approx 1.6$ is the dynamical exponent. Thus, just as observed for the ion beam nanopatterning, the relative variation of $\tau(q)$ is *less* than the relative variation in $I(q)$. At large Δt , the KPZ dynamics exhibits stretched exponential behavior [30]. However, for small Δt , the leading terms in the relaxation are those of a compressed exponential [31] and simulations are also fit well with compressed exponential behavior [32]. These suggest an effective exponent $n \approx (2 + 2\alpha)/z \approx 1.74$ [31]. This exponent value is, in fact, at least approximately equal to that observed at the nanoripple wavenumber peaks $\pm q_0$ in these experiments. There have been extensive studies of temporal and spatial persistence in the KPZ and other growth models using different metrics than measured by speckle correlation experiments. It would be interesting to expand theoretical inquiry into the persistence of surface morphology itself, as measured in these experiments.

This material is based on work supported by the National Science Foundation (NSF) under Grant No. DMR-1709380. X.Z. and R.H. were supported by the U.S. Department of Energy (DOE) Office of Science under Grant No. DE-SC0017802. Experiments were performed at the Coherent Hard X-ray (CHX) beamline at National Synchrotron Light Source II (NSLS-II), a U.S. Department of Energy (DOE) Office of Science User Facility operated for the DOE Office of Science by Brookhaven National Laboratory under Contract No. DE-SC0012704. We thank Glenn Thayer and Heitor Mourato of the Boston University Scientific Instrumentation Facility for design and construction of the sample holder.

-
- [1] M. Sutton, *Comptes rendus physique* **9**, 657 (2008).
- [2] A. Madsen, A. Fluerasu, and B. Ruta, *Synchrotron light sources and free-electron lasers*, 1 (2015).
- [3] P. De Gennes, *Physica* **25**, 825 (1959).
- [4] B. J. Berne and R. Pecora, *Dynamic light scattering: with applications to chemistry, biology, and physics* (Courier Corporation, 2000).
- [5] G. Williams and D. C. Watts, *Transactions of the Faraday society* **66**, 80 (1970).
- [6] B. Bagchi and S. Bhattacharyya, *Advances in chemical physics* **116**, 67 (2001).
- [7] S. A. Norris, J. C. Perkinson, M. Mokhtarzadeh, E. Anzenberg, M. J. Aziz, and K. F. Ludwig, *Scientific reports* **7**, 2016 (2017).
- [8] J. C. Perkinson, J. M. Swenson, A. DeMasi, C. Wagenbach, K. F. Ludwig Jr, S. A. Norris, and M. J. Aziz, *Journal of Physics: Condensed Matter* **30**, 294004 (2018).
- [9] G. Santoro and S. Yu, *X-ray Scattering*, 1 (2017).
- [10] S. Sinha, E. Sirota, S. Garoff, and H. Stanley, *Physical Review B* **38**, 2297 (1988).
- [11] O. Bikondoa, D. Carbone, V. Chamard, and T. H. Metzger, *Scientific reports* **3**, 1850 (2013).
- [12] M. Mokhtarzadeh, J. G. Ulbrandt, P. Myint, S. Narayanan, R. L. Headrick, and K. F. Ludwig Jr, *Physical Review B* **99**, 165429 (2019).
- [13] R. Gago, L. Vázquez, R. Cuerno, M. Varela, C. Ballesteros, and J. M. Albella, *Nanotechnology* **13**, 304 (2002).
- [14] M. Engler, S. Macko, F. Frost, and T. Michely, *Physical Review B* **89**, 245412 (2014).
- [15] T. Basu, D. P. Datta, and T. Som, *Nanoscale research letters* **8**, 289 (2013).
- [16] D. A. Pearson and R. M. Bradley, *Journal of Physics: Condensed Matter* **27**, 015010 (2014).
- [17] K. F. Ludwig Jr, C. Eddy Jr, O. Malis, and R. Headrick, *Applied physics letters* **81**, 2770 (2002).
- [18] O. Bikondoa, *Journal of applied crystallography* **50**, 357 (2017).
- [19] M. P. Harrison, D. A. Pearson, and R. M. Bradley, *Physical Review E* **96**, 032804 (2017).
- [20] B. Wu, T. Iwashita, and T. Egami, *Physical review letters* **120**, 135502 (2018).
- [21] J.-P. Bouchaud, *Anomalous Transport*, 327 (2008).
- [22] L. Cipelletti and L. Ramos, *Journal of Physics: Condensed Matter* **17**, R253 (2005).
- [23] B. Ruta, Y. Chushkin, G. Monaco, L. Cipelletti, E. Pineda, P. Bruna, V. Giordano, and M. Gonzalez-Silveira, *Physical review letters* **109**, 165701 (2012).
- [24] A.-D. Brown and J. Erlebacher, *Physical Review B* **72**, 075350 (2005).
- [25] A.-D. Brown, J. Erlebacher, W.-L. Chan, and E. Chason, *Physical review letters* **95**, 056101 (2005).
- [26] F. Livet, F. Bley, R. Caudron, E. Geissler, D. Abernathy, C. Detlefs, G. Grübel, and M. Sutton, *Physical Review E* **63**, 036108 (2001).
- [27] A. Fluerasu, M. Sutton, and E. M. Dufresne, *Physical review letters* **94**, 055501 (2005).
- [28] K. Ludwig, F. Livet, F. Bley, J.-P. Simon, R. Caudron, D. Le Bolloch, and A. Moussaid, *Physical Review B* **72**, 144201 (2005).
- [29] M. Kardar, G. Parisi, and Y.-C. Zhang, *Physical Review Letters* **56**, 889 (1986).
- [30] F. Colaiori and M. Moore, *Physical Review E* **63**, 057103 (2001).
- [31] E. Katzav and M. Schwartz, *Physical Review E* **69**, 052603 (2004).
- [32] M. Mokhtarzadeh and K. F. Ludwig Jr, *Journal of synchrotron radiation* **24**, 1187 (2017).